Monatsh Chem (2010) 141:529–537
DOI 10.1007/s00706-010-0288-2

ORIGINAL PAPER

Kinetics of Ag/TiO_2-photocatalyzed iodide ion oxidation

Chockalingam Karunakaran · Premkumar Anilkumar · Paramasivan Gomathisankar

Received: 4 December 2009 / Accepted: 25 February 2010 / Published online: 2 April 2010

Abstract Ag-doped TiO_2 (anatase) samples (mass fraction $w_{Ag} = 0.01$ and $w_{Ag} = 0.02$) of 15.9 and 14.5 nm mean particle size and 11.46 and 10.14 $m^2\ g^{-1}$ BET surface area were prepared by photodeposition. Doping results in surface plasmon resonance of the metallic silver nanoclusters at around 500 nm, but the absorption edge remains unaltered at 365 nm. Ag-doping remarkably enhances the photooxidation of iodide ion under UV light; iodine formation with Ag/TiO_2 with $w_{Ag} = 0.01$ is 16 times greater than with bare TiO_2. The reaction conforms to Langmuir–Hinshelwood kinetics with regard to both I^- and O_2. Increase of pH slows down iodine formation and sacrificial electron donors arrest the reaction. Pre-sonication of the catalyst slurry hinders the photocatalysis. Generation of iodine is much greater in acetonitrile than in water. Under the experimental conditions, Ag/TiO_2 with $w_{Ag} = 0.01$ is more efficient than Ag/TiO_2 with $w_{Ag} = 0.02$, and the enhanced photocatalysis is likely to be because of suppression of electron–hole pair recombination. Kinetic analysis reveals that increasing the Ag mass fraction from 0.01 to 0.02 enhances the surface pseudo-first-order rate constant but inhibits the adsorption of iodide ion and the oxygen molecule on the illuminated oxide surface.

Keywords Ag-doped TiO_2 · Photochemistry · Catalysis · Surface · Nanoparticles

C. Karunakaran (✉) · P. Anilkumar · P. Gomathisankar
Department of Chemistry, Annamalai University,
Annamalainagar 608002, Tamilnadu, India
e-mail: karunakaranc@rediffmail.com

Introduction

Shining semiconductors with light of energy equal to or larger than the band gap creates electron-hole pairs, holes in the valence band and electrons in the conduction band. Whereas a fraction of these pairs reach the crystal surface and react with adsorbed substrates, leading to photocatalysis, the rest recombine resulting in low photocatalytic efficiency [1]. TiO_2 is a promising candidate for photocatalytic material application because of its exceptional optical and electronic properties, chemical stability, non-toxicity, and low cost [2, 3]. Also, water is adsorbed on TiO_2, both molecularly and dissociatively [4, 5], and hole trapping by either the surface hydroxyl groups or the adsorbed water molecules generates short-lived HO· radicals, which are the primary oxidizing agents in the photomineralization of organics [6–9]. The high density of surface hydroxyl groups on the TiO_2 particle may also be the reason for the observed high photocatalytic activity of TiO_2 [10]. However, the high degree of recombination between the photogenerated electrons and holes is a major factor reducing photocatalytic efficiency. The photocatalytic efficiency of TiO_2 can be improved by doping it with a noble metal such as silver [11–18]. The metal particles deposited on the surface of TiO_2 may act as sink for the photogenerated electrons and thus reduce electron–hole recombination. This migration of the conductance-band electrons to metal particles increases the lifetime of the holes and thus the photocatalytic efficiency. Investigations with Ag-doped TiO_2 as photocatalyst are many but they are on the degradation of organics [11–18]. Moreover, there is no report on the kinetics of $Ag–TiO_2$ photocatalysis and hence this study was conducted. Generation of energy-bearing chemicals by nonspontaneous reactions is the objective of solar energy conversion and storage, and

iodide ion oxidation is such a reaction ($\Delta G^\circ = +51.6$ kJ mol^{-1}). Further, the operational efficiency of the iodide–triiodide redox couple affects the light-to-electricity conversion efficiency of dye-sensitized solar cells [19]. The mechanism of TiO_2-photocatalyzed iodide ion oxidation has been studied in detail [20, 21], and, besides TiO_2 [20–28], MoO_3, Fe_2O_3, ZnO, and CeO_2 [22–24] have also been tested as photocatalysts for iodide ion oxidation.

This study reveals the effect of Ag composition on the photoadsorption of iodide ion and the oxygen molecule on the oxide surface and the velocity of the surface reaction.

Results and discussion

Catalyst characterization

The XRD pattern of undoped TiO_2 is identical with the standard pattern of anatase (JCPDS 01-078-2486 C), and the rutile lines (01-089-0553 C) are absent. This clearly reveals that the TiO_2 used for doping is of the anatase phase. The X-ray diffraction patterns of the prepared Ag–TiO_2 samples match that of the undoped TiO_2 and are identical with the JCPDS pattern of anatase (Fig. 1). These results confirm that photodeposition of the silver does not modify the basic crystal structure of the TiO_2 used (tetragonal, $a = 0.37845$ nm, $c = 0.95143$ nm, body centered). The diffraction patterns of the Ag/TiO_2 samples do not show XRD peaks of metallic silver at 38.2° (111), 44.4° (200), etc. (JCPDS 03-092). This may be because of either homogeneous dispersion of discrete silver deposits on the nanoscale on the surface of the TiO_2 or because the silver content is so low it is difficult to detect. The energy dispersive X-ray spectroscopic studies confirm the presence of silver deposits on TiO_2 (Fig. 2). Further, determination of the silver content of the prepared Ag/TiO_2 samples by EDX spectroscopic analysis is in agreement with the weight percentages of silver in the Ag/TiO_2 samples. Particle size determination by light scattering shows that the prepared Ag/TiO_2 catalysts are nanoparticles. Peak analysis (by number) provides the mean particle sizes of Ag/TiO_2 as 15.9 nm ($w_{Ag} = 0.01$) and 14.5 nm ($w_{Ag} = 0.02$), the detailed distributions are shown in Fig. 3. N_2 adsorption and desorption studies show the isotherms as type II (Fig. 4). This type of isotherm is indicative of nonporous materials. Surface area measurements, made by the BET method, provide the specific surface areas of Ag/TiO_2 as 11.46 m^2 g^{-1} ($w_{Ag} = 0.01$) and 10.14 m^2 g^{-1} ($w_{Ag} = 0.02$). Determination of the specific pore volume of both Ag/TiO_2 samples (0.032 and 0.020 cm^3 g^{-1} for $w_{Ag} = 0.01$ and $w_{Ag} = 0.02$, respectively), show that the

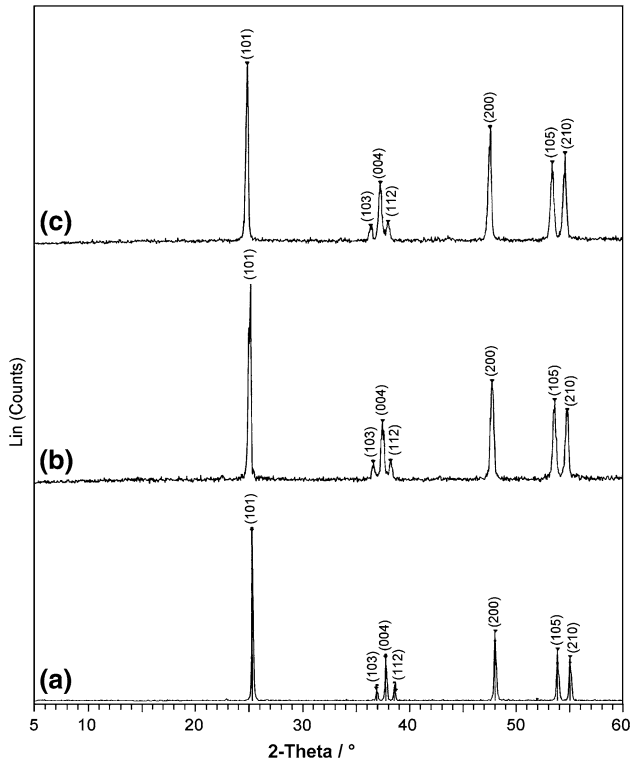

Fig. 1 XRD patterns of **a** undoped TiO_2, **b** Ag/TiO_2 with $w_{Ag} = 0.01$, and **c** Ag/TiO_2 with $w_{Ag} = 0.02$; the *inverted triangles* denote JCPDS 01-078-2486 C: anatase

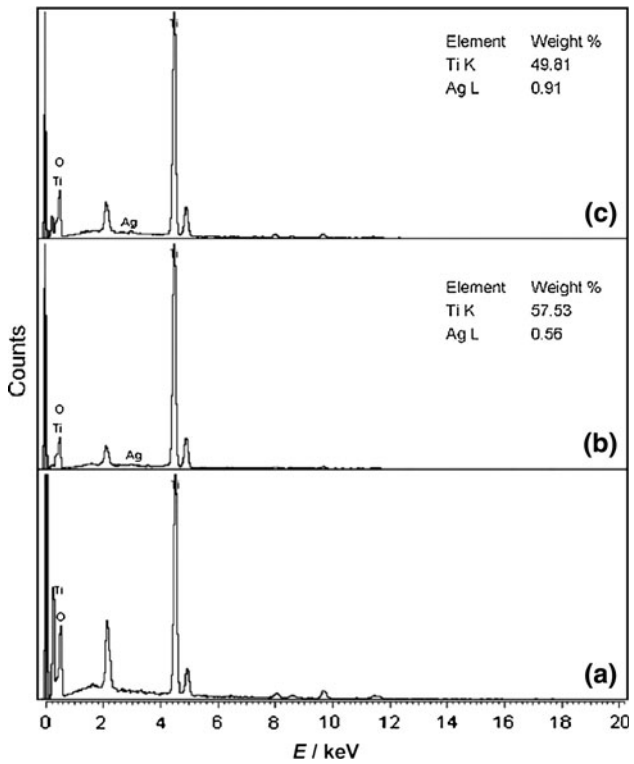

Fig. 2 EDX patterns of **a** undoped TiO_2, **b** Ag/TiO_2 with $w_{Ag} = 0.01$, and **c** Ag/TiO_2 with $w_{Ag} = 0.02$

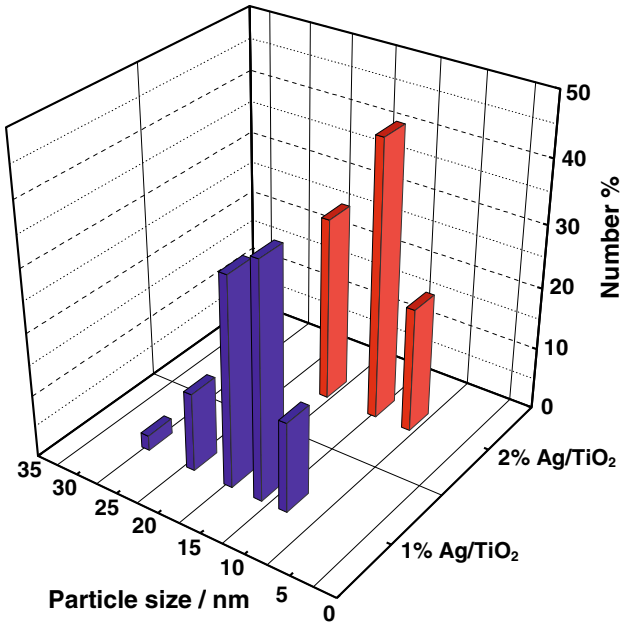

Fig. 3 Particle size

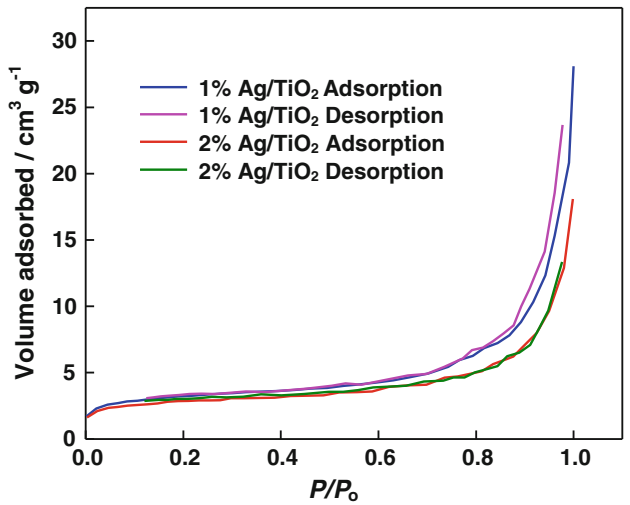

Fig. 4 BET isotherms of Ag/TiO_2 with $w_{Ag} = 0.01$ and $w_{Ag} = 0.02$

prepared catalysts are nonporous. The scanning electron micrographs of undoped TiO_2 and the Ag/TiO_2 samples, given in Fig. 5, reveal globular morphology of the particles. It is interesting to note that there is no obvious change in the morphology of the support TiO_2 because of silver doping. The silver particles deposited on TiO_2 could not be detected by SEM even at 50,000 resolution, indicating the nanodimensions of the silver deposits on the TiO_2. The diffuse reflectance spectra (DRS) of bare TiO_2 and the Ag/TiO_2 ($w_{Ag} = 0.01$ and 0.02) are presented in Fig. 6. Comparison of the DRS of Ag/TiO_2 and bare TiO_2 shows that deposition of the silver does not significantly change the band gap. However, to obtain more precise band edges

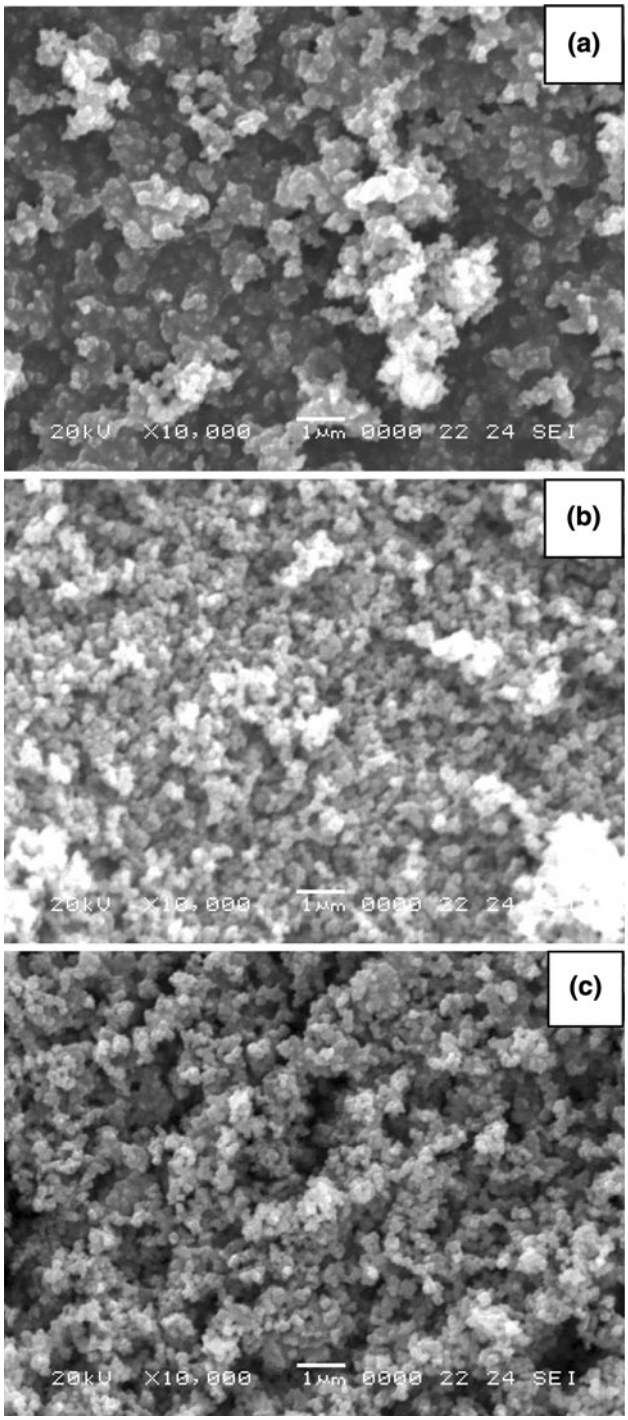

Fig. 5 SEM images of **a** undoped TiO_2, **b** Ag/TiO_2 with $w_{Ag} = 0.01$, and **c** Ag/TiO_2 with $w_{Ag} = 0.02$

of the undoped TiO_2 and Ag/TiO_2 samples the differential diffuse reflectance spectra were obtained. The band edges of bare TiO_2, Ag/TiO_2 with $w_{Ag} = 0.01$, and Ag/TiO_2 with $w_{Ag} = 0.02$, as seen in differential diffuse reflectance spectra, are 368, 365, and 365 nm, respectively. The broad absorption around 500 nm exhibited by the Ag/TiO_2

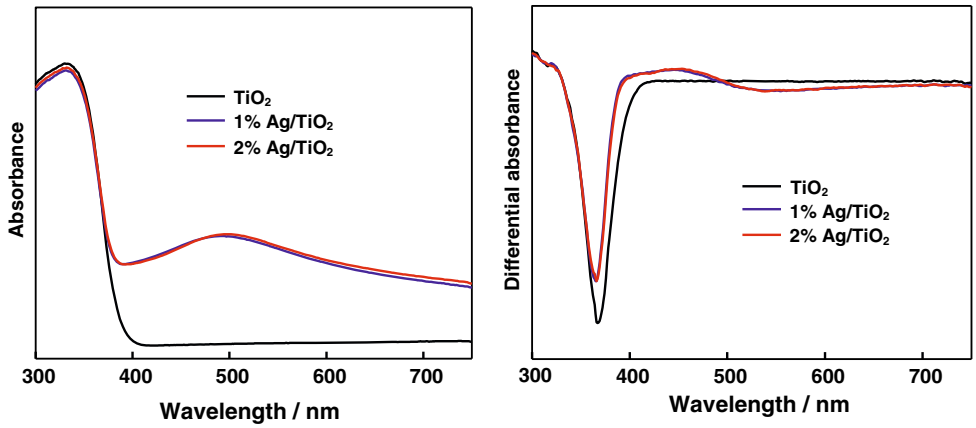

Fig. 6 DRS of undoped and Ag-doped TiO_2

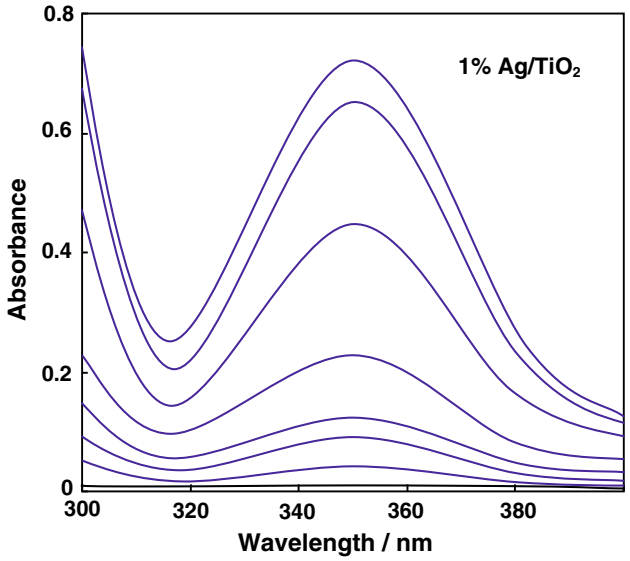

Fig. 7 Ag/TiO_2 ($w_{Ag} = 0.01$)-catalyzed iodine generation under UV light. The UV–Vis spectra of KI solution, diluted ten times, was recorded at 0, 5, 10, 15, 30, 60, 90, and 120 min (*from bottom to top*). Catalyst loading = 0.020 g, $[I^-] = 0.050$ M, dissolved $O_2 = 22.4$ mg dm^{-3}, airflow rate = 7.8 dm^3 s^{-1}, $\lambda = 365$ nm, photon flux = 25.2 μEinstein dm^{-3} s^{-1}, iodide solution = 25 cm^3

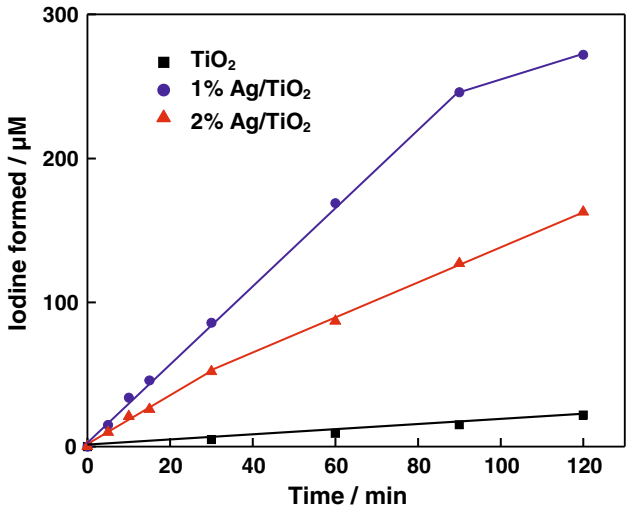

Fig. 8 Iodine generation by undoped and Ag-doped TiO_2 under UV light. Catalyst loading = 0.020 g, $[I^-] = 0.050$ M, dissolved $O_2 = 22.4$ mg dm^{-3}, airflow rate = 7.8 cm^3 s^{-1}, $\lambda = 365$ nm, photon flux = 25.2 μEinstein dm^{-3} s^{-1}, iodide solution = 25 cm^3

samples is attributed to the surface plasmon resonance of metallic silver nanoparticles deposited on the TiO_2 surface [13, 15, 29, 30]. The color of Ag/TiO_2 also suggests that the silver is mainly in the metallic state.

Photooxidation of iodide ion

In aqueous suspension, the prepared Ag/TiO_2 samples ($w_{Ag} = 0.01$ and $w_{Ag} = 0.02$) effectively catalyze the oxidation of iodide ion under illumination at 365 nm. The UV–Vis spectrum of the KI solution, illuminated with Ag/TiO_2, displays the generation of iodine ($\lambda_{max} = 350$ nm); the spectrum is similar to that of the authentic iodine–iodide solution (Fig. 7). Chemical tests also confirm iodine formation: the solution turns purple with starch and the color is discharged by thiosulfate. The oxidation does not take place in the dark. Also, the photogeneration of iodine is insignificant in absence of the catalysts. Further, analytical experiments show that AgI is not formed during the photocatalysis. The photocatalytic efficiencies of the silver-deposited TiO_2 samples are far higher than that of the undoped TiO_2 (Fig. 8). Here, it is pertinent to state that the degradation of rhodamine B dye under UV light is only slightly enhanced by deposition of silver on TiO_2 [17]. Photocatalysis by Ag/TiO_2 with $w_{Ag} = 0.01$ slackens after 90 min whereas that by Ag/TiO_2 with $w_{Ag} = 0.02$ slows down after 30 min. The slackening of iodine generation under continuous illumination is not unknown; similar results have been observed in the oxidation of iodide ion

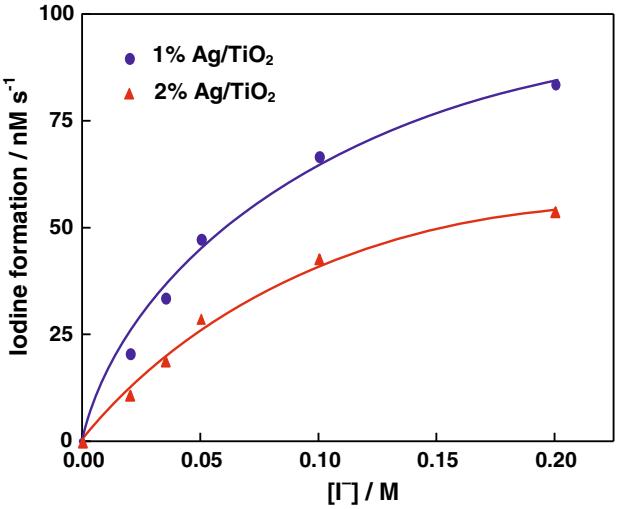

Fig. 9 Dependence of iodine generation on iodide ion concentration. Catalyst loading = 0.020 g, dissolved O_2 = 22.4 mg dm^{-3}, airflow rate = 7.8 cm^3 s^{-1}, λ = 365 nm, photon flux = 25.2 μEinstein dm^{-3} s^{-1}, iodide solution = 25 cm^3, illumination = 30 min

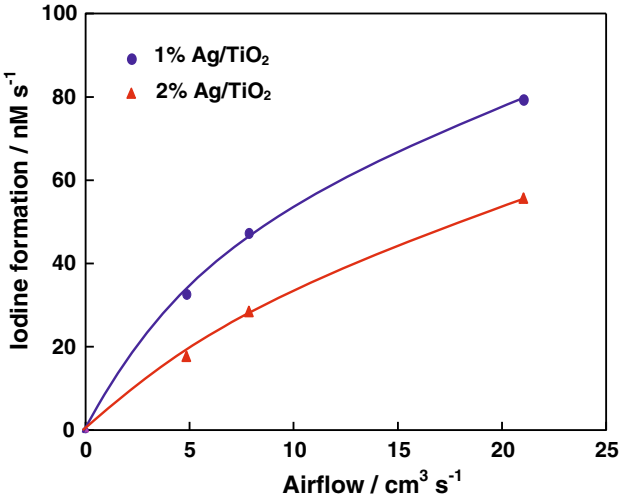

Fig. 10 Dependence of iodine formation on airflow rate. Catalyst loading = 0.020 g, [I^-] = 0.050 M, λ = 365 nm, photon flux = 25.2 μEinstein dm^{-3} s^{-1}, iodide solution = 25 cm^3, illumination = 30 min

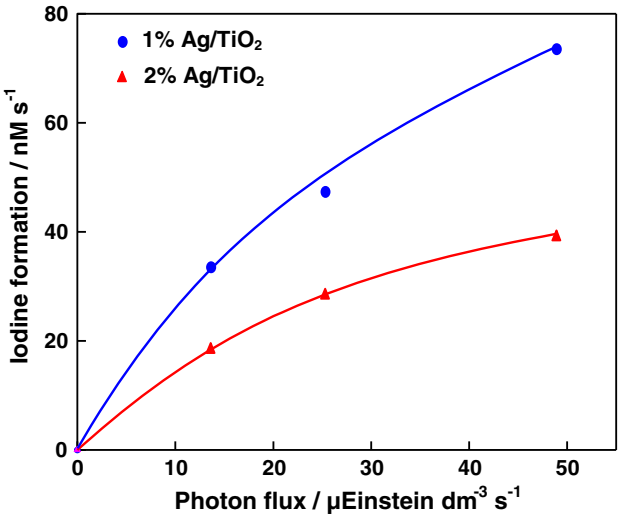

Fig. 11 Iodine formation as a function of light intensity. Catalyst loading = 0.020 g, [I^-] = 0.050 M, dissolved O_2 = 22.4 mg dm^{-3}, airflow rate = 7.8 cm^3 s^{-1}, λ = 365 nm, iodide solution = 25 cm^3, illumination = 30 min

elsewhere [22, 23, 26, 27], and nonnegligible photoreduction of iodine on the TiO_2 surface at appreciable iodine concentration is the probable reason [20]. Because iodine formation with both catalysts is not slowed down up to at least half-an-hour of illumination, the initial rates of iodine liberation were obtained by estimating the iodine formed after illumination for half-an-hour; the results were reproducible to ±4%. Both catalysts exhibit sustainable photocatalytic activity; recycling of the used catalysts without pretreatment yields identical results. Rate measurements at different concentrations of iodide ion show Langmuir–Hinshelwood kinetics (Fig. 9). Study of the photoreaction as a function of airflow rate reveals enhancement of photocatalysis by oxygen, and variation of the rate of iodine generation with airflow also conforms to Langmuir–Hinshelwood kinetics (Fig. 10). The photogeneration of iodine was studied as a function of photon flux and Fig. 11 presents the enhancement of iodine formation with light intensity. The photooxidation of iodide ion on both catalysts slows with increasing pH. Figure 12 shows the variation of the rates of iodine formation with pH; the pH of the KI solution was varied by addition of NaOH or HCl and measured after allowing the slurry to attain equilibrium. The plausible reason for the slowdown of iodine formation with increasing pH is the increasing adsorption of hydroxyl ion on the Ag/TiO_2 surface. The medium turning basic may result in enhanced adsorption of hydroxyl ion on the catalyst surface thereby making the surface more negatively charged. Negatively charging the Ag/TiO_2 particles reduces the adsorption of iodide ion and thus the oxidation.

The photooxidation of iodide ion with light of wavelength 365 and 254 nm, carried out separately using the micro reactor but under identical conditions, shows that UV-C light is more effective than UV-A light at generating iodine (Table 1). The possible reason for greater iodide ion oxidation under illumination at 254 nm than at 365 nm is that the iodine formed also absorbs at 365 nm. That is, the liberated iodine may screen the catalyst by absorbing part of the illumination thereby reducing the intensity of the light impinging on the catalyst. Sacrificial electron donors, for example trimethylamine and hydroquinone (5 mM) arrest the photooxidation of iodide ion on Ag/TiO_2 (conditions as in Fig. 8). Vinyl monomer acrylonitrile also arrests the photooxidation, indicating the involvement of a

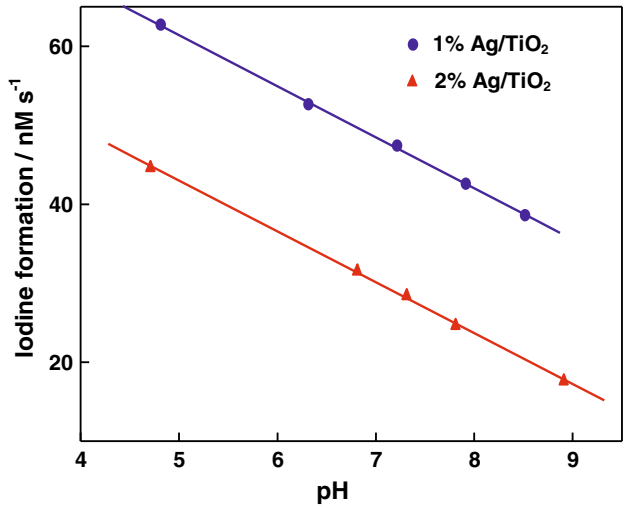

Fig. 12 Variation of iodine generation with pH. Catalyst loading = 0.020 g, $[I^-] = 0.050$ M, dissolved $O_2 = 22.4$ mg dm^{-3}, airflow rate = 7.8 cm^3 s^{-1}, $\lambda = 365$ nm, photon flux = 25.2 μEinstein dm^{-3} s^{-1}, iodide solution = 25 cm^3, illumination = 30 min

Table 1 Iodine formation under UV-A and UV-C light

λ (nm)	I_2 formation (nM s^{-1})	
	Ag/TiO_2 ($w_{Ag} = 0.01$)	Ag/TiO_2 ($w_{Ag} = 0.02$)
365[a]	34	14
254[b]	137	53

10 cm^3 0.05 M KI, 0.020 g catalyst loading, 7.8 cm^3 s^{-1} airflow, 22.4 mg dm^{-3} dissolved O_2, 30 min illumination, 6 W

[a] 18.4 μEinstein dm^{-3} s^{-1}

[b] 6.2 μEinstein dm^{-3} s^{-1}

chain carrier in the photocatalysis. The photooxidation of iodide ion both in tubular and in immersion reactors with 25 and 250 cm^3 KI solutions, respectively, show greater formation of iodine with the latter, indicating the possibility of scaling up the process (Table 2). Sonication results in surface and particle size modification of the catalyst [31] and the photocatalytic activity is susceptible to modification of the surface and size of the catalyst particles. In this study, pre-sonication of the Ag/TiO_2 ($w_{Ag} = 0.01$ and $w_{Ag} = 0.02$) slurries in KI solution for 10 min at 37 ± 3 kHz and 100 W suppresses the photocatalytic activity; iodine generation by pre-sonicated Ag/TiO_2 is less than that by the unsonicated material (Table 3). On pre-sonication the Ag/TiO_2 slurry turns puffy, which may be the reason for inactivation of the surface. The active silver nanoclusters on the surface of TiO_2 could be buried because of sonication. Enhancing the efficiency of photocatalysis, especially in the formation of energy-bearing chemicals by thermodynamically uphill reactions, is of prime concern in solar energy conversion and storage, and our experiments with the prepared Ag/TiO_2 ($w_{Ag} = 0.01$ and $w_{Ag} = 0.02$) in acetonitrile reveal enhanced photoformation of iodine; Table 3 shows larger formation of iodine in acetonitrile than in water. A possible explanation for the higher photocatalytic efficiency of Ag/TiO_2 in acetonitrile than in aqueous suspension is the absence of hole-capture by the hydroxyl ions and water molecules in acetonitrile medium.

Table 2 Iodine formed in tubular and immersion photoreactors in 30 min

Reactor	I_2 generated (μmol)	
	Ag/TiO_2 ($w_{Ag} = 0.01$)	Ag/TiO_2 ($w_{Ag} = 0.02$)
Tubular[a]	1.9	1.0
Immersion[b]	10.8	5.9

0.05 M KI, 0.020 g catalyst loading, 7.8 cm^3 s^{-1} airflow, 22.4 mg dm^{-3} dissolved O_2, 365 nm

[a] 25.2 μEinstein dm^{-3} s^{-1}, 25 cm^3 KI solution

[b] 33.9 μEinstein dm^{-3} s^{-1}, 250 cm^3 KI solution

Kinetic analysis

The Langmuir–Hinshelwood kinetic model is applicable to semiconductor photocatalysis and the kinetic law is [24, 32]:

$$\text{rate} = kK_1K_2I^mCS[I^-]\gamma/(1 + K_1[I^-])(1 + K_2\gamma)$$

where K_1 and K_2 are the adsorption coefficients of iodide ion and molecular oxygen on the illuminated surface of the catalyst, k is the surface pseudo-first-order rate constant, S is the specific surface area of the catalyst, C is the catalyst loading per liter, γ is the airflow rate, I is the light intensity per liter (in Einstein dm^{-3} s^{-1}) and m is an exponent with a value of unity at low light flux but falling to 0.5 at high light flux [33, 34]. At a given iodide ion concentration, $K_1[I^-]/(1 + K_1[I^-])$ is a constant and the Langmuir–Hinshelwood kinetic model holds good, as seen from the data fit to the curve governed by the kinetic equation and drawn using computer software [32] (Fig. 10). Further, at a fixed airflow rate, $K_2\gamma/(1 + K_2\gamma)$ is also a constant and Fig. 9

Table 3 Enhanced Ag/TiO_2 photocatalysis in acetonitrile

Solvent	I_2 formation (nM s^{-1})	
	Ag/TiO_2 ($w_{Ag} = 0.01$)	Ag/TiO_2 ($w_{Ag} = 0.02$)
Water	43 (34)	22 (13)
Acetonitrile	110	50

25 cm^3 0.05 M KI, 0.020 g catalyst loading, 7.8 cm^3 s^{-1} airflow, 25.2 μEinstein dm^{-3} s^{-1} at 365 nm for 30 min; values in parentheses correspond to pre-sonication for 10 min at 37 ± 3 kHz and 100 W

Table 4 The kinetic constants

Catalyst	m	K_1 (dm^3 mol^{-1})	K_2 (cm^{-3} s)	k (μmol m^{-2} $Einstein^{-1}$)
Ag–TiO_2 ($w_{Ag} = 0.01$)	0.6	10.2	0.078	24
Ag–TiO_2 ($w_{Ag} = 0.02$)	0.6	6.3	0.030	44

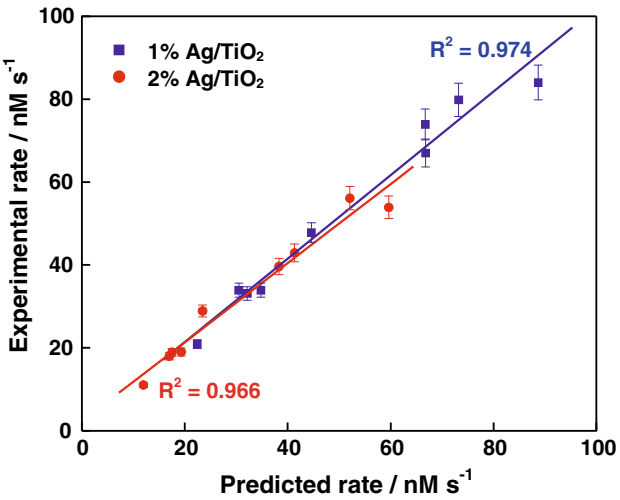

Fig. 13 Graphical display of Ag–TiO_2-photocatalyzed iodine formation data fit

shows that the results conform to the Langmuir–Hinshelwood kinetics. The kinetic constants deduced from the fits are presented in Table 4, and Fig. 13 is the graphical display of the data fit using the listed kinetic constants; the experimental results are plotted against those predicted on the basis of the kinetic law. Comparison of the K_1 and K_2 values of Ag-doped TiO_2 ($w_{Ag} = 0.01$ and $w_{Ag} = 0.02$) shows that increasing the Ag-doping inhibits the adsorption of iodide ion and molecular oxygen on the illuminated TiO_2 surface and this may be one of the reasons for the lower photocatalytic activity of Ag–TiO_2 with $w_{Ag} = 0.02$. Table 4 also shows that the m values of Ag–TiO_2 with $w_{Ag} = 0.01$ and 0.02 are the same. This indicates that the UV light absorptivity of both doped oxides does not differ significantly. Table 4 also reveals that doping enhances the surface pseudo-first-order rate constant (k); this may be because of the larger suppression of the photogenerated electron–hole recombination.

Mechanism of enhanced photocatalysis

Comparison of the rates of photoformation of iodine on the undoped and Ag-doped TiO_2 shows that the deposition of small amounts of silver metal on the TiO_2 surface leads to a large increase in photocatalytic efficiency (Fig. 8).The DRS of bare TiO_2 and Ag/TiO_2 reveal that the band gap of TiO_2 is not changed by deposition of silver (Fig. 6), hence the enhanced photocatalytic activity of Ag/TiO_2 particles under UV light is not because of its band gap energy. The Ag/TiO_2 samples exhibit surface plasmon resonance around 500 nm because of the deposited metallic silver nanoparticles [13, 15, 30] (Fig. 6). The surface plasmon resonance of silver particles, which can be excited by visible light, increases the electric field around metal particles and thus enhances surface electron excitation and electron–hole separation on silver-deposited TiO_2 particles [17]. However, the absorption band of the plasmon resonance is not strong, probably because of the low silver content, and hence its contribution could be significant only under visible light; the silver surface plasmon resonance is not excited by UV light [17]. Silver particles deposited on the surface of TiO_2 can act as electron–hole separation centers [12, 15, 17, 29]. Because the Fermi level of silver is lower than that of TiO_2 the movement of photogenerated electrons from the conduction band of TiO_2, leaving behind the holes in the valence band, to the silver particles deposited on the surface of TiO_2 is thermodynamically feasible [15, 16, 29, 30]. This migration of the generated electrons to metal particles can suppress the fast electron–hole recombination and increase the lifetime of the holes. The difference between the Fermi levels results in the formation of a Schottky barrier at the Ag–TiO_2 interface, which promotes the charge separation [15, 16, 29, 30]. That is, the transferred electrons are trapped by metallic silver, because of its strong electron-accepting ability, resulting in the effective separation of the electrons and holes. Accordingly, more electrons and holes can be produced, leading to enhanced quantum efficiency of photocatalysis. Further, the deposition of silver has a positive effect on the scavenging of the photogenerated electrons by O_2 [17]. The rate-determining step in photocatalytic oxidation on TiO_2 is believed to be electron transfer from the TiO_2 surface to the adsorbed O_2, whereas in Ag/TiO_2-photocatalyzed oxidation electron transfer is from the metallic silver to O_2; the detailed mechanism of semiconductor-photocatalyzed iodide ion oxidation has been discussed elsewhere [10, 21–25].

Comparison of the photocatalytic activity of Ag/TiO_2 with $w_{Ag} = 0.01$ and $w_{Ag} = 0.02$ under all the experimental conditions, reveals that Ag/TiO_2 with $w_{Ag} = 0.01$ is more efficient than Ag/TiO_2 with $w_{Ag} = 0.02$. Beyond the optimum level of silver loading, the big metal particles formed on the surface of TiO_2 attract more electrons and

become new recombination centers of photogenerated electrons and holes [12, 17, 30]. This reduces the efficiency of charge separation. Superfluous silver doping leads to occupation of more active sites on the surface of TiO_2, which also reduces the photoinduced efficiency [18, 30]. Further, higher loading of silver reduces the photocatalytic activity because of blocking of incident light by the overcoated silver grains [12, 15, 18].

Conclusions

Ag/TiO_2 (anatase) with $w_{Ag} = 0.01$ and 0.02, prepared by photoreduction of Ag^+ on TiO_2 and characterized by XRD, SEM, EDX, etc., are of spherical morphology with mean particle size and BET surface area of 15.9 and 14.5 nm, and 11.46 and 10.14 $m^2\ g^{-1}$, respectively. The deposition of silver on TiO_2 does not change the band gap energy although surface plasmon resonance at around 500 nm results, because of the presence of metallic silver nanoparticles on the TiO_2. The prepared Ag/TiO_2 samples have remarkably high photocatalytic efficiency in the oxidation of iodide ion under UV light and under the experimental conditions the efficiency of Ag/TiO_2 with $w_{Ag} = 0.01$ is greater than that of Ag/TiO_2 with $w_{Ag} = 0.02$. Iodine liberation conforms to the Langmuir–Hinshelwood kinetic model and slows down with increasing pH. Sacrificial electron donors, for example trimethylamine, arrest the oxidation and iodine liberation is high in acetonitrile. The higher efficiency of iodine formation under illumination at 254 nm than at 365 nm is likely to be because of the absorbance of the incident UV-A light by the iodine formed. Experiments in tubular and immersion reactors show the possibility of scaling up the process. Sonication reduces the photocatalytic efficiency of Ag/TiO_2, probably by burying the silver nanoclusters. The improved photocatalytic efficiency of Ag/TiO_2 is likely to be because of suppression of the recombination of the photogenerated electron–hole pairs. Kinetic analysis shows that increasing the Ag content enhances the surface reaction but inhibits adsorption of iodide ion and oxygen molecules on the surface.

Experimental

Materials

TiO_2, $AgNO_3$, and KI, supplied by Merck (India), were of analytical grade. Methanol and acetonitrile, also of analytical grade, were distilled before use. De-ionized distilled water was used throughout the study.

Catalyst preparation

The Ag/TiO_2 samples ($w_{Ag} = 0.01$ and $w_{Ag} = 0.02$) were prepared by photodeposition. TiO_2 (1.0 g) was suspended in 100 cm^3 water containing 0.0157 or 0.0315 g $AgNO_3$ and 1 or 2 cm^3 methanol, and air was purged through the solution continuously [11, 12]. Under magnetic stirring, the solution was illuminated for 8 h at 365 nm with eight 8-W mercury lamps. The completion of silver deposition on TiO_2 was confirmed by analytical methods; the catalyst was separated by centrifugation, washed with water, and dried at 100 °C.

Characterization

The powder XRD patterns were recorded with a Bruker D8 system using Cu K_α radiation of wavelength 0.15406 nm in a 2θ range of 5-60° at a scan speed of 0.050° s^{-1}. The morphology of the oxide was determined with a JEOL JSM-5610 scanning electron microscope (SEM) equipped with BE detector. The sample was placed on an adhesive carbon slice supported on copper stubs and, before measurement, coated with 10 nm thick gold using a JEOL JFC-1600 auto fine coater. A JEOL JSM-5610 SEM equipped with EDX was used for the energy dispersive X-ray spectroscopic studies. The specific surface areas of the catalysts were determined using a Micromeritics ASAP 2020 sorption analyzer. The samples were degassed at 423 K for 12 h, and analysis was performed at 77 K with N_2 gas as the adsorbate. The Brunauer–Emmett–Teller (BET) multipoint method least-square fit provided the specific surface area. A Shimadzu UV-2450 spectrometer was employed with $BaSO_4$ as reference to record the UV–Vis diffuse reflectance spectra of the oxides.

Photoreactors

A multilamp photoreactor, fitted with eight 8-W mercury lamps of wavelength 365 nm (Sankyo Denki, Japan) and a highly polished anodized aluminium reflector, was used to carry out the detailed photocatalytic study; the reaction vessel was a borosilicate glass tube of 15 mm inner diameter and was placed at the center. The four cooling fans at the bottom of the reactor dissipate the heat generated. The light intensity was varied by using two, four, or eight lamps with angles subtended at the sample by adjacent lamps of 180°, 90°, and 45°, respectively. A micro photoreactor fitted with a 6-W, 254 nm low-pressure mercury lamp and a 6-W, 365 nm mercury lamp was also used to carry out the photoreaction. Quartz and borosilicate glass tubes were used as reaction vessels for 254 and 365 nm lamps, respectively. The photooxidation was also performed in an immersion type reactor fitted with a 125-

W medium-pressure mercury lamp of wavelength 365 nm and a highly polished anodized aluminium reflector. The reaction vessel was a 500 cm^3 double-walled borosilicate immersion well with inlet and outlet for water circulation. The light intensities under all experimental conditions were determined by ferrioxalate actinometry [35].

Photooxidation

For each experiment a fresh solution of KI of the required concentration was prepared and the photooxidation was carried out with 25, 10, and 250 cm^3 of the solution in the multilamp, micro, and immersion photoreactors, respectively. Air was bubbled through the solution, which effectively kept the added catalyst under suspension and in continuous motion; the airflow rate was determined by the soap bubble method. After illumination, the catalysts were recovered by centrifugation and the iodine formed was estimated spectrophotometrically at 350 nm; calibration curves were constructed using standard iodine–iodide solutions [22–24]. A time lag of at least 15 min was provided before illumination to ensure pre-adsorption of iodide ion and oxygen molecules on the catalyst surface. The dissolved oxygen was measured using an Elico dissolved oxygen analyzer PE 135.

Acknowledgments Financial support through research grant no. F.12-64/2003 (SR) by the University Grants Commission (UGC), New Delhi, is thankfully acknowledged, and P.A. is grateful to UGC for PF.

References

1. Thompson TL, Yates JT Jr (2006) Chem Rev 106:4428
2. Gaya UI, Abdullah AH (2008) J Photochem Photobiol C 9:1
3. Diebold U (2003) Surf Sci Rep 48:53
4. Osgood R (2006) Chem Rev 106:4379
5. Zhao J, Li B, Onda K, Feng M, Petek H (2006) Chem Rev 106:4402
6. Shiraishi Y, Saito N, Hirai T (2005) J Am Chem Soc 127:12820
7. Peller J, Wiest O, Kamat PV (2004) J Phys Chem A 108:10925
8. Du Y, Rabani J (2003) J Phys Chem B 107:11970
9. Sun L, Bolton JR (1996) J Phys Chem 100:4127
10. Linsebigler AL, Lu G, Yates JT Jr (1995) Chem Rev 95:735
11. Bansal A, Madhavi S, Tan TTY, Lim TM (2008) Catal Today 131:250
12. Young C, Lim TM, Chiang K, Scott J, Amal R (2008) Appl Catal B 78:1
13. Sa J, Fernandez-Garcia M, Anderson JA (2008) Catal Commun 9:1991
14. Paramasivam I, Macak JM, Schmuki P (2008) Electrochem Commun 10:71
15. Seery MK, George R, Floris P, Pillai SC (2007) J Photochem Photobiol A 189:258
16. Lee MS, Hong SS, Mohseni M (2005) J Mol Catal A 242:135
17. Sung-Suh HM, Choi JR, Hah HJ, Koo SM, Bae YC (2004) J Photochem Photobiol A 163:37
18. Trans H, Scott J, Chiang K, Amal R (2006) J Photochem Photobiol A 183:41
19. Zhang Z, Ito S, Moser JE, Zakeeruddin SM, Gratzel M (2009) ChemPhysChem 10:1834
20. Green ANM, Chandler RE, Haque SA, Nelson J, Durrant JR (2005) J Phys Chem B 109:142
21. Fitzmaurice DJ, Eschie M, Frei H (1993) J Phys Chem 97:3806
22. Karunakaran C, Anilkumar P (2008) Solar Energy Mater Solar Cells 92:490
23. Karunakaran C, Anilkumar P (2007) J Mol Catal A 265:153
24. Karunakaran C, Senthilvelan S, Karuthapandian S, Balaraman K (2004) Catal Commun 5:283
25. Ishibashi K-I, Fujishima A, Watanabe T, Hashimoto K (2000) J Photochem Photobiol A 134:139
26. Ohno T, Fujihara K, Saito S, Matsumura M (1997) Solar Energy Mater Solar Cells 45:169
27. Hodak J, Quinteros C, Litter MI, Roman ES (1996) J Chem Soc Faraday Trans 92:5081
28. Tennakone K, Kumarasinghe AR, Kumara GRRA, Wijayantha KGU, Sirimanne PM (1997) J Photochem Photobiol A 108:193
29. Zhang L, Yu JC (2005) Catal Commun 6:684
30. Zhang F, Pi Y, Cui J, Yang Y, Zhang X, Guan N (2007) J Phys Chem C 111:3756
31. Hirano K, Nitta H, Sawada K (2005) Ultrason Sonochem 12:271
32. Karunakaran C, Senthilvelan S, Karuthapandian S (2005) J Photochem Photobiol A 172:207
33. Vincze L, Kemp TJ (1995) J Photochem Photobiol A 87:257
34. Karunakaran C, Sujatha MP, Gomathisankar P (2009) Monatsh Chem 140:1269
35. Kuhn HJ, Braslavsky SE, Schmidt R (2004) Pure Appl Chem 76:2105